Biosensors and Bioelectronics 52 (2014) 445–451

Contents lists available at ScienceDirect

Biosensors and Bioelectronics

journal homepage: www.elsevier.com/locate/bios

Magnetoresistive sensor for real-time single nucleotide polymorphism genotyping

Giovanni Rizzi, Frederik Westergaard Østerberg, Martin Dufva, Mikkel Fougt Hansen *

Department of Micro- and Nanotechnology, Technical University of Denmark, DTU Nanotech, Building 345 East, DK-2800 Kongens Lyngby, Denmark

ARTICLE INFO

Article history:
Received 8 July 2013
Received in revised form
15 August 2013
Accepted 3 September 2013
Available online 19 September 2013

Keywords:
Biosensor
Magnetoresistive sensor
Single nucleotide polymorphism
Microfluidics
DNA genotyping

ABSTRACT

We demonstrate a magnetoresistive sensor platform that allows for the real-time detection of point mutations in DNA targets. Specifically, we detect point mutations at two sites in the human beta globin gene. For DNA detection, the present sensor technology has a detection limit of about 160 pM and a dynamic range of about two orders of magnitude. The sensors are based on a new geometry for biological sensing that detects the difference between the amount of beads bound to a sensing pad and a local integrated negative reference pad. The magnetic beads are magnetised by the magnetic field arising from the sensor bias current such that no external magnetic fields are needed. The sensors are integrated in a microfluidic system with temperature control. The local negative reference integrated in the sensor geometry efficiently compensates for sensor offsets, external magnetic fields and a uniform background of magnetic beads, which enables real-time quantification of the specific binding of magnetic beads to the sensor surface under varying experimental conditions.

1. Introduction

Genotyping has wide application in diagnostics of genetic diseases, cancers, and viral and bacterial infections. There is an ever-increasing need for rapid, specific and sensitive methods to detect particular DNA sequences in a sample. Several diseases are related to alternative forms (alleles) of a given gene. For cancer and genetic diagnostics, the assays must be able to distinguish DNA species differing in only one base to perform so called single nucleotide polymorphism (SNP) genotyping. In some cases the SNP is known and specific probes against that particular SNP can be designed. In other cases, the SNP is unknown and must be screened for. Allele specific hybridisation is a rapid method for SNP genotyping that employs probes specific for the wild type (WT) and mutant type (MT) sequences. A simple hybridisation and dehybridisation reaction, most often with an end-point fluorescence readout, can then be used to obtain specificity. Multiplexing allele specific reactions is a substantial optimisation process and sequence dependent variation around each respective SNP makes it difficult to obtain fully optimised SNP calling at a given assay condition (Poulsen et al., 2011). The efficacy of SNP calling can be increased by treating the hybridisation at different stringencies by varying the salt concentration or the temperature (Howell et al., 1999; Poulsen et al., 2011; Petersen et al., 2008, 2009). The SNP calling can be performed after a given time point or in real time (Howell et al., 1999; Poulsen et al., 2011; Petersen et al., 2008, 2009). Studying real-time dehybridisation is preferable since far more conditions can be investigated as compared to post washing analysis. However, real-time fluorescence monitoring is hampered by high background signals from the fluorochromes used to detect the hybrids. Real-time investigation of hybridisation and dehybridisation can also be used to obtain high resolution melting curves for screening of unknown mutations in a sample (Er and Chang, (2012)). Such analyses are mostly performed in solution phase using intercalating fluorescent dyes. A corresponding analysis is possible using DNA microarrays (Nørholm et al., 2004), but it requires specialised and bulky instrumentation, and it is still hampered by high background signals from fluorochromes present in the sample.

Biosensors with a readout based on the binding of magnetic beads to the surface of a magnetoresistive field sensor based on the giant magnetoresistance (GMR) or tunnelling magnetoresistance effects have been proposed for the detection of DNA or proteins by a number of authors and are reviewed by Freitas et al. (2007), Tamanaha et al. (2008) and Wang and Li (2008). Common for most of these approaches is that the magnetic beads are excited by an oscillating applied magnetic field resulting in a signal detectable by the magnetic field sensor. The studies have focused on the end-point detection by comparing the signal level after a washing step to that before the sample was introduced. Recently, Gaster et al. (2009) demonstrated the first real-time measurements of the magnetic bead-binding to a GMR sensor surface due to protein interactions. These measurements were

* Corresponding author. Tel.: +45 45 25 63 38.
E-mail address: Mikkel.Hansen@nanotech.dtu.dk (M. Fougt Hansen).

0956-5663/$ - see front matter © 2013 Elsevier B.V. All rights reserved.
http://dx.doi.org/10.1016/j.bios.2013.09.026

carried out in a background of magnetic beads and thus the need for washing was eliminated. Although the magnetoresistive sensing technology is promising, real-time measurements of the binding due to specific biological interactions have been limited to protein interactions.

In the present work, we demonstrate a novel magnetoresistive-based sensor architecture that allows for real-time detection of microarray-based DNA hybridisation and dehybridisation without the issues of washing steps and measurement of the background signal.

Previously, we have presented the design of magnetic field sensors in a planar Hall effect cross-geometry (Ejsing et al., 2004) and a Wheatstone bridge geometry based on the anisotropic magnetoresistance effect (Henriksen et al., 2010). The particular Wheatstone bridge configuration studied by Henriksen et al. (2010) gave the same response as the planar Hall effect sensor cross geometry except for a geometrical amplification factor and was hence named planar Hall effect bridge (PHEB) geometry. It has been demonstrated that sensors based on this geometry are well suited for dynamic measurements on magnetic beads in a liquid volume near the sensor surface using only the magnetic field from the sensor bias current as excitation (Østerberg et al., 2013a). Here, we present a new Wheatstone bridge sensor geometry, which integrates a local negative reference. We show that this enables the real-time quantification of beads that are *specifically* bound to the sensor surface due to biomolecular recognition, even in a background of magnetic beads in suspension and when the environmental conditions of the sensor are changed. Subsequently, we evaluate the sensitivity of the present sensors when used for DNA analysis and demonstrate their applicability for SNP detection.

2. Material and methods

2.1. Sensor designs

The PHEB sensors are based on the anisotropic magnetoresistance of a thin film of permalloy ($Ni_{80}Fe_{20}$) of the Wheatstone bridge geometry shown in Fig. 1a, which is exchange-pinned along the x-direction using an antiferromagnetic layer (Henriksen et al. (2010)). When biased with an AC voltage $V_x = \sqrt{2}\, V_{RMS}\, \sin(2\pi f t)$, a magnetic field H_y acting on the sensor area along the y-axis gives rise to a sensor voltage output along the y-axis, which can be measured by lock-in detection in the first harmonic in-phase signal. For small fields, the response is linear and given by $V_1' = (V_{RMS}/R) S_0 H_y$, where R is the bridge resistance and $S_0 (< 0)$ is the low-field sensitivity (see Supplementary Material). The current running in the sensor also generates a small inhomogeneous magnetic field in the proximity of the sensor surface (Hansen et al., 2010; Østerberg et al., 2013b). This self-field is used to magnetise the magnetic beads near the surface allowing for their detection with no need for external magnetic fields. The signal from magnetic beads over the sensor surface can be measured by lock-in detection in the second harmonic out-of-phase signal (Østerberg et al., 2013a), which can be written as

$$V_2'' = -\frac{1}{4} S_0 \left(\frac{V_{RMS}}{R}\right)^2 (\gamma_0 + \gamma_1) \tag{1}$$

A detailed derivation of this expression is given in the Supplementary Material. Here, γ_0 is a constant describing a sensor self-biasing due to current shunting in other layers than the magnetoresistive layer and γ_1 is a parameter accounting for the signal due to magnetic beads, which depends on the sensor width, the bead diameter, the bead magnetic susceptibility and the bead number density distribution in the volume over the sensor (including both beads on the sensor surface and in the volume over the sensor) (Hansen et al., 2010). The value of γ_1 is zero in the absence of magnetic beads and positive in the presence of magnetic beads.

Here, we propose a new sensor geometry termed differential PHEB (dPHEB) with identical top and bottom halves of the bridge as illustrated in Fig. 1b. This symmetry makes the sensor nominally insensitive to uniform magnetic fields. Moreover, since the self-field acts identically on the top and bottom parts, the second harmonic out-of-phase signal depends *only* on differences in the amount of beads on and over the top and bottom halves of the bridge, respectively. The second harmonic out-of-phase signal of the dPHEB sensor can be expressed as

$$V_2'' = -\frac{1}{8} S_0 \left(\frac{V_{RMS}}{R}\right)^2 (\gamma_{top} - \gamma_{bottom}) \tag{2}$$

where S_0 is the low-field sensitivity of a PHEB sensor with identical dimensions and γ_{top} and γ_{bottom} depend on the amount of beads on and over the top and bottom halves of the bridge. If the bead concentration in the liquid over the sensor surface is the same for the two sensor halves, only a difference in the amount of surface-bound magnetic beads is anticipated to give rise to a difference between γ_{top} and γ_{bottom}. A full derivation of Eq. (2) is given in the Supplementary Material. In this work, only the top half of the differential sensor is functionalised to allow for cancellation of the signal from the beads in suspension.

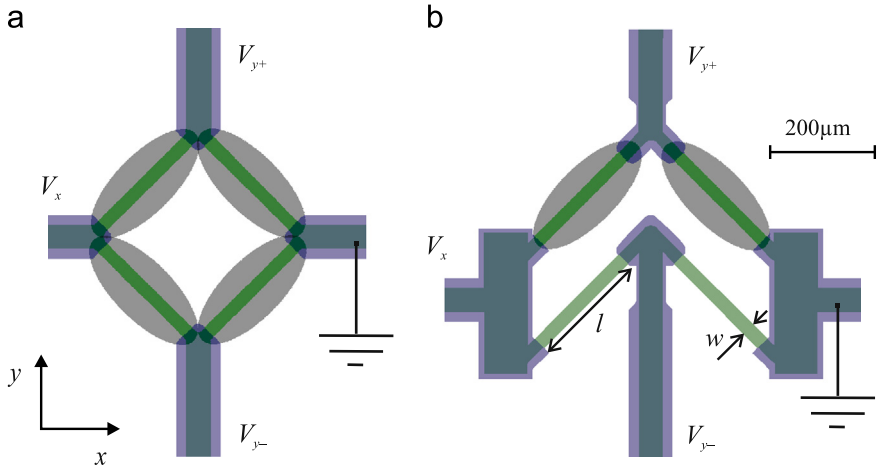

Fig. 1. Schematic illustration of sensor geometries: (a) PHEB sensor (b) Differential PHEB (dPHEB) sensor. The sensors are voltage-biased along the x-axis and the sensor signal V_y is measured along the y-axis. The arms of the sensor bridges are functionalised with surface-linked probes as indicated by the grey areas.

2.2. Sensor fabrication

The magnetic field sensors with the geometries in Fig. 1 with $l = 250\ \mu m$ and $w = 25\ \mu$m were fabricated as described previously by Henriksen et al. (2010). Briefly, the top-pinned magnetic stack Ta(15)/$Ni_{80}Fe_{20}$(30)/$Mn_{80}Ir_{20}$(10)/Ta(5) (all thicknesses in nm) was deposited by sputtering in a saturating magnetic field applied along the *x*-direction. Compared to our previous studies, the stack was slightly modified to have a thicker bottom tantalum layer and a thinner Mn–Ir layer to reduce the sensor self-biasing (γ_0). The electrical contacts consisting of Ti(10)/Pt(100)/Au(100)/Ti (10) were deposited by electron beam evaporation and defined by lift-off. The sensors were passivated with a layer of Ormocomp (Micro resist technology GmbH, Berlin, Germany) hybrid polymer of thickness 900 nm. The polymer, diluted 1:2 in Ma-T 1050, was spin coated over the sensors at 3000 rpm for 60 s. The coating geometry was defined by UV lithography and after development, the polymer was hard baked for 3 h at 150 °C. Finally, the wafer was diced into chips, each comprising six sensors.

2.3. Surface chemistry and patterning

A silanisation of the sensor surface was used to covalently couple amino-labelled oligonucleotides to the sensor coating. Briefly, this was carried out by: (1) surface activation for 20 min in 45% H_2O_2 followed by rinsing in MilliQ water and drying; (2) washing in acetone and dipping in 10% v/v solution of 3-Aminopropyltriethoxysilane (APTS) in acetone for 30 min; (3) rinsing in acetone and drying followed by immersion in 5% v/v solution of Glutaraldehyde (GA) in MilliQ water for 30 min; (4) rinsing in MilliQ water and drying.

Solutions of 20 μM capture probe oligonucleotides in 3 × saline-sodiumcitrate (SSC) (Invitrogen, Auckland, New Zealand) were spotted on the sensor surface to cover the sensor arms as depicted in Fig. 1 using a Nanoplotter™ with a NanoTip™ (both from GeSim GmbH, Grosserkmannsdorf, Germany) and incubated overnight.

In this work we used allele-specific DNA probes (Supplementary Table S2) designed for SNP genotyping in the human beta globin (*HBB*) gene by Petersen et al. (2008). Two mutation sites were investigated: CD 8/9 and CD 17. The wild type (WT) and mutant type (MT) probes differ by a single base insertion (CD 8/9) and by a single base substitution (CD 17), respectively. In addition, a biotinylated probe was used as a direct binding site for magnetic labels to function as a positive reference. All probes were purchased from DNA Technology A/S, Risskov, Denmark.

Prior to use, the sensors were rinsed in MilliQ water and the surface was blocked in a solution of 1 mg/mL bovine serum albumin (BSA) in 1 × phosphate buffered saline (PBS) for 20 min.

2.4. Measurement platform

The chip was mounted in a click-on microfluidic system (Østerberg et al., 2010) ensuring electrical contacts to the sensors, and defining a fluidic channel ($1 \times 1 \times 5\ mm^3$) over the chip surface. The sensors were connected in parallel and a voltage $V_{RMS} = 1.6$ V at a frequency $f = 167$ Hz was applied by the lock-in amplifier via a commercial audio amplifier. This frequency was chosen low enough to ensure that the magnetic response of the beads was in-phase with the field excitation and high enough to facilitate low-noise measurements at a rate of about 3 data points per second. The resistance of a single sensor bridge was $R = 89\ \Omega$, such that the *RMS* bridge current was 18 mA. The corresponding *RMS* value of the magnetic excitation field at the surface of the sensor was about 0.25 mT (see Supplementary Material).

The sensor signals were amplified using SR552 bipolar preamplifiers and measured with SR830 lock-in amplifiers from Stanford Research Systems Inc, Sunnyvale, CA, USA. The temperature of the chip holder was measured with a Pt1000 thermoresistor and controlled using a Peltier element with an accuracy of 0.1 °C via an LFI3751 temperature controller (Wavelength Electronics, Inc., Bozeman, MT, USA).

The response of the two sensor designs to a homogeneous external applied magnetic field was measured in the first harmonic in-phase sensor voltage V_1'. The magnetic field, provided by a custom built Helmholtz coil, was swept in steps from +11 mT to −11 mT and back. These measurements were used to obtain the low-field sensitivity for the PHEB sensor and to test the immunity of the dPHEB sensor to a homogeneous external applied magnetic field.

The response of the sensor designs to magnetic beads magnetised by the sensor self-field was measured in the second harmonic out-of-phase signal V_2'' in zero external applied magnetic field. To compensate for small offsets in the V_2'' signals, the experimental results are plotted as the variations $\Delta V_2''$ of the V_2'' signals with respect to their values at the initiation of the experiment.

2.5. Experimental procedure

2.5.1. Target oligonucleotides and magnetic labels

The target oligonucleotides (Supplementary Table S2) were 120 bases long synthetic sequences from the human *HBB* gene (DNA Technology A/S, Risskov, Denmark). Probes towards the CD 8/9 and CD 17 mutation sites (Supplementary Table S2) were biotinylated in the 5' end to allow for binding to the streptavidin coated magnetic labels.

The magnetic beads used for this work were Miltenyi Streptavidin MicroBeads (Cat. 130-048-102, Miltenyi Biotec Norden AB, Lund, Sweden) with a nominal diameter of 50 nm. According to Gaster et al., 2011, each bead comprises on the order of ten iron oxide nanoparticles with a diameter of about 10 nm.

2.5.2. Sensitivity to magnetic beads

Here, we linked biotinylated DNA probes directly to the sensor surface and studied the sensor output change for the two sensor types upon exposure to streptavidin magnetic beads as function of the number of functionalised sensor arms (see Supplementary Fig. S4a for a schematic illustration).

In the experiments, 15 μL of stock solution of streptavidin magnetic beads was injected over the functionalised sensor by means of a syringe pump and the variation of the second harmonic signal ($\Delta V_2''$) after 20 min of incubation was recorded. Subsequently, the sensors were washed with 1 × PBS at a flow rate of 200 μL/min for 1 min and the sensor signals were measured again.

2.5.3. DNA hybridisation and dose-response

Here, we formed a sandwich between DNA capture probes immobilised on the sensor surface, the biotinylated DNA target and streptavidin magnetic beads and studied the time response vs. the DNA target concentration (see Supplementary Fig. S4b for a schematic illustration).

In the experiments, we used a dPHEB sensor functionalised on the top two arms with CD 8/9 WT capture probes. The biotinylated WT target was diluted in 2 × SSC + 0.05% SDS in a five-fold dilution series and mixed 1:1 v/v with the stock magnetic bead suspension to final DNA target concentrations ranging from 40 nM to 0.156 nM. Immediately after, 20 μL of sample was injected into the microfluidic sensor at a flow rate of 30 μL/min and incubated for 60 min at 37 °C under stagnant conditions. The change of the

second harmonic out-of-phase signal ($\Delta V_2''$) was monitored vs. time during the incubation.

2.5.4. Real-time SNP genotyping

Here, we studied the response of dPHEB sensors functionalised with DNA capture probes upon exposure to DNA target–bead mixtures during incubation under low stringency conditions and subsequently under higher stringency washing (see Supplementary Fig. S4c for a schematic illustration).

The top arms of two sensors on the same chip were functionalised with WT and MT capture probes, respectively. The two mutation sites were investigated on separate chips. Solutions of 10 nM WT, MT or 1:1 mixture of MT/WT DNA were prepared in 1 × SSC+0.025% SDS. 10 μL of the target solution was mixed with 10 μL of the stock bead solution and immediately injected into the microfluidic sensor system at a flow rate of 30 μL/min. The final concentration of the target was 5 nM and the buffer was 0.5 × SSC+0.012% SDS. The sample was incubated over the sensor for 30 min at 37 °C. After hybridisation, the sensors were washed with 0.05 × SSC+0.05% SDS for 80 s at a flow rate of 30 μL/min and left stagnant. Three repetitions of the procedure were performed for each target combination. The sensor signals were monitored real-time during the process.

To compare the signals from the two sensors, we define the normalised ratio (*NR*) of the sensor signals as

$$NR = \frac{\Delta V_2''[WT]}{\Delta V_2''[WT] + \Delta V_2''[MT]}, \quad (3)$$

where $\Delta V_2''[WT]$ and $\Delta V_2''[MT]$ are the second harmonic out-of-phase signal variations for the sensors functionalised with WT and MT capture probes, respectively.

3. Results

3.1. Sensitivity to external fields and magnetic beads

First, the response of the two sensor designs in Fig. 1 to external magnetic fields was compared. The inset of Fig. 2 shows the first harmonic in-phase signal (V_1') measured as function of homogeneous external applied magnetic fields $\mu_0 H_y$ in the range ± 11 mT. The standard PHEB sensor showed the behaviour described previously (Henriksen et al., 2010) with a linear low-field region with a slope corresponding to a low-field sensitivity of $S_0/\mu_0 \cong -300$ V/(AT). The response of the differential sensor (dPHEB) was about 50 times smaller. This shows that the differential sensor efficiently cancelled out homogeneous externally applied magnetic fields as well as the sensor self-bias field.

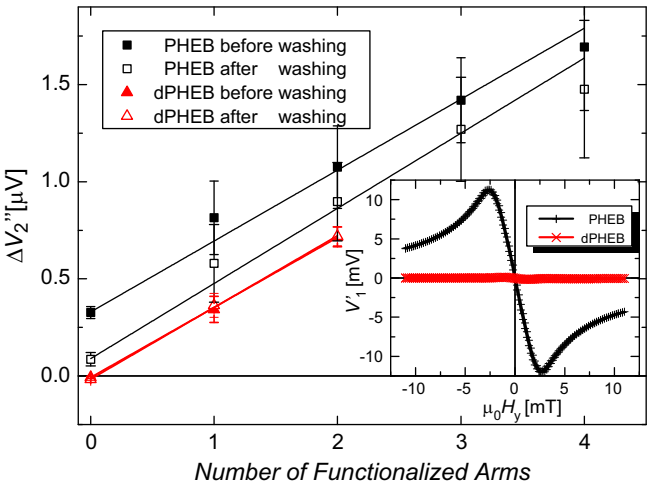

Fig. 2. Second harmonic out-of phase signal $\Delta V_2''$ vs. number of sensor arms functionalised with biotinylated positive reference probes. The signals before washing were measured with the magnetic bead suspension in the microfluidic channel over the sensor. The signals after washing were obtained with no beads in the liquid channel after washing with 1 × PBS. Error bars are standard deviations obtained from repeated experiments ($n=3$). *Inset*: First harmonic in-phase signal vs. external applied magnetic field $\mu_0 H_y$ in the range ± 11 mT.

Subsequently, the response of the two sensor designs was investigated as function of the number of sensor arms functionalised with a biotinylated capture probe upon exposure to streptavidin coated magnetic beads.

The squares in Fig. 2 show the signal measured for PHEB sensors as function of the number of arms functionalised with biotinylated capture probes before and after washing, respectively. Note, that the measurements before washing were carried out with the magnetic bead suspension in the liquid channel over the sensor. The signal was found to increase linearly with the number of functionalised arms. This shows that the signals from the arms are additive in accordance with the theory presented in the Supplementary Material. Moreover, before washing a significant signal was observed from the arms with no functionalisation. Washing was found to significantly reduce but not eliminate this signal. The signal vs. number of functionalised arms was observed to follow a straight line with the same slope but different non-zero offsets both before and after washing.

The triangles in Fig. 2 show the corresponding signals measured for dPHEB sensors when zero to two of the upper sensor arms were functionalised as illustrated in Fig. 1b. In this case, no offset of the sensor response vs. number of functionalised arms was observed and the points measured before and after washing (i.e., with and without beads in the fluid channel) were perfectly overlapping with the same slope as observed for the PHEB sensors. Moreover, the standard deviations on the measurements on the dPHEB sensors were found to be about four times smaller than those obtained for the PHEB sensors.

3.2. DNA hybridisation and dose-response curve

A dPHEB sensor was functionalised on the two top arms with CD 8/9 WT capture probe oligonucleotides as illustrated in the inset of Fig. 3. In the assay, the biotinylated WT target of different concentrations was mixed with the streptavidin magnetic beads and introduced into the fluidic system to form the WT capture probe – biotinylated WT target – streptavidin magnetic bead sandwich on the sensor

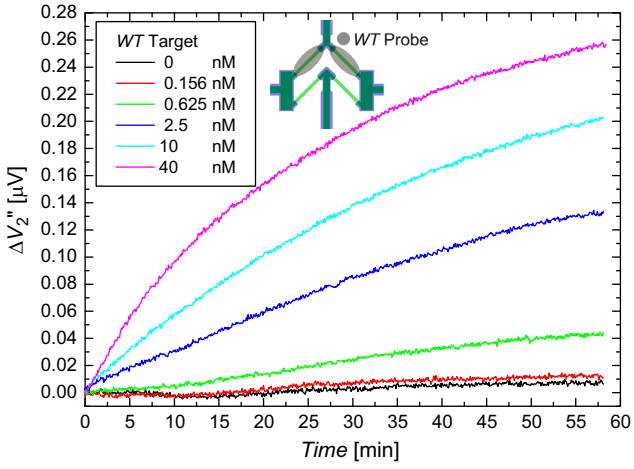

Fig. 3. Second harmonic out-of-phase signal variation measured during incubation of biotinylated WT target of the indicated concentrations and streptavidin coated magnetic beads with dPHEB sensors functionalised with CD 8/9 WT capture probe oligonucleotides as illustrated in the inset. The target and beads entered the fluidic system at time $t=0$ min.

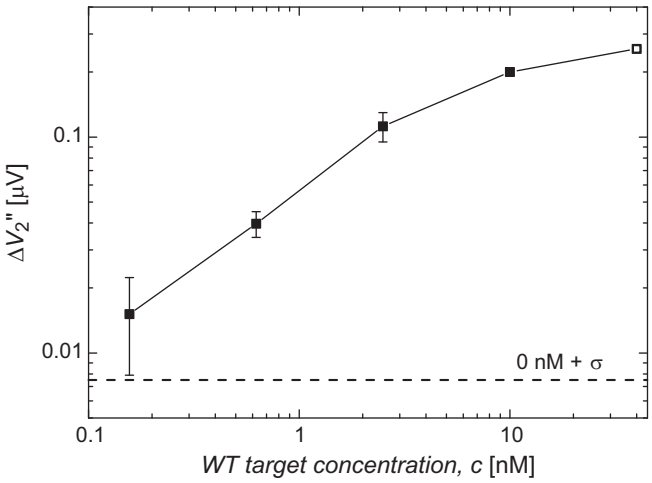

Fig. 4. Signal variation vs. WT target concentration from dPHEB sensors functionalised with CD 8/9 WT capture probe oligonucleotides after about 60 min of hybridisation with the WT target and streptavidin magnetic beads. Error bars are standard deviations obtained from repeated experiments ($n=3$), except for c=40 nM ($n=1$). The dashed line indicates the negative control result plus one standard deviation ($n=3$).

surface. Fig. 3 shows the measured signal variation $\Delta V_2''$ vs. time t during incubation with the bead-WT target mixture.

The dPHEB geometry allowed us to follow the hybridisation reaction in real-time. After sample injection, the signal increased for all tested target concentrations with a tendency to level off for long times (this was most pronounced for the highest tested concentration). The no DNA target sample showed only a small variation of the signal around 0 μV (Fig. 3). These small signal fluctuations were around two times the noise of the sensor signal, and determined our limit of detection. The smallest investigated concentration ($c=156$ pM) gave a signal still discernible from the negative reference. Fig. 4 shows the relationship between the target concentration and the signal measured after about 60 min of hybridisation. The dashed line indicates the mean value of three reference experiments with no DNA ($\Delta V_2''=4.5$ nV) plus one standard deviation ($\sigma=3.1$ nV). The signal for the lowest tested concentration was above this threshold level. The signal for the sample with the highest target concentration ($c=40$ nM) reached $\Delta V_2'' = 0.25\ \mu V$ corresponding to about one third of the value obtained when the biotinylated DNA was directly linked to the sensor surface (Fig. 2). This difference may be due to the higher affinity of the streptavidin–biotin bond and the more complex reaction dynamics when both the target and the beads are in suspension compared to when only the beads are in suspension. The signal in Fig. 4 starts to saturate when the target concentration exceeds about 10 nM and hence the readout has a dynamic concentration range of about two orders of magnitude.

3.3. Real-time SNP genotyping

In these experiments, the arms of two different dPHEB sensors on the same chip were functionalised with WT and MT capture probes as illustrated in the inset of Fig. 5. The two mutation sites (CD 8/9 and CD17) were investigated on separate chips. Real-time measurements of the sensor signals were performed during incubation with the streptavidin bead—biotinylated DNA mixtures (compositions given in the figure) as well as during subsequent washing with a higher stringency buffer. The target concentration was chosen to 5 nM to ensure that the signal was close to but below saturation such that dehybridisation events could be maximally resolved. The measured signals for the individual sensors are shown vs. time in Supplementary Fig. S5. The resulting normalised ratios *NR* given by Eq. (3) for three repetitions of the

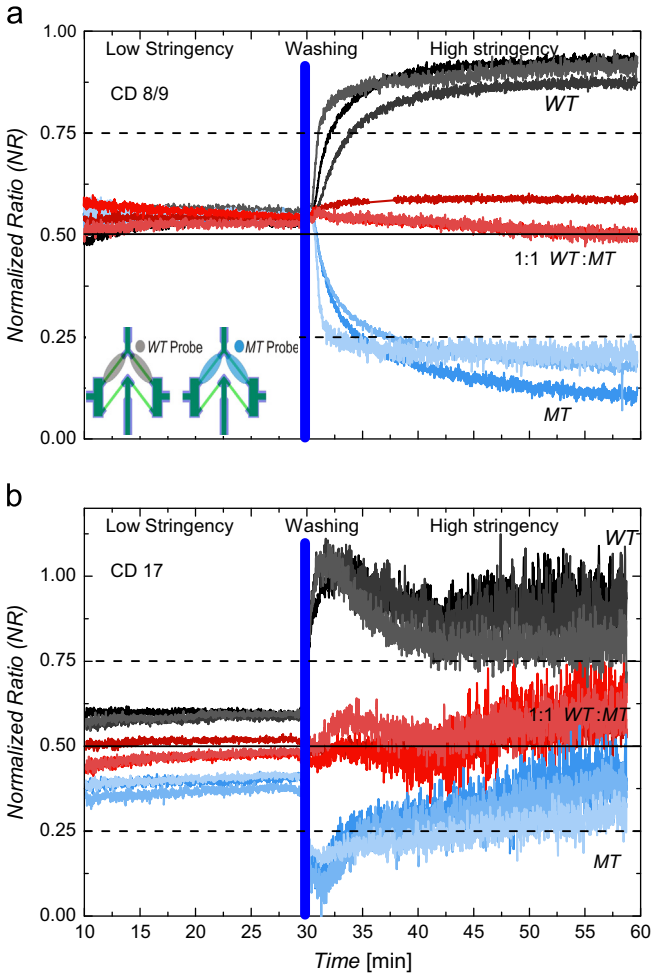

Fig. 5. Normalised signal ratio (NR) vs. time for experiments with the indicated target combinations. The sensors were functionalised with WT and MT capture probes as depicted in the inset for (a) the CD 8/9 mutation site and (b) the CD 17 mutation site in the human HBB gene, respectively. Samples were injected at $t=0$ min. The normalised ratio was not meaningful for the first 10 min due to low signals.

indicated target compositions are shown in Fig. 5a and b for the CD 8/9 and CD 17 mutation sites, respectively. Values of *NR* of 1 and 0 correspond to hybridisation to only the WT and MT capture probes, respectively, and $NR=0.5$ corresponds to identical hybridisation to the two probes.

For the CD 8/9 mutation site, after approximately 15 min of hybridisation under low stringency condition (0.5 × SSC+0.012% SDS), the normalised ratio approached 0.5 for all target combinations, corresponding to identical hybridisation of all targets to WT and MT capture probes (Figs. 5a and 6a). For all target combinations, we found $NR \cong 0.54(1)$.

For the CD 17 mutation site, the value of the normalised ratio prior to washing was found to differ for the three target combinations (Figs. 5b and 6a) and the signal level was generally lower than for the CD 8/9 mutation (Supplementary Fig. S5). For the three targets we found $NR \cong 0.39(2)$ (MT target), $NR \cong 0.49(2)$ (1:1 WT:MT target) and $NR \cong 0.591(6)$ (WT target), respectively.

Under higher stringency conditions (0.05 × SSC+0.05% SDS), the mismatched duplexes denatured at a faster rate than the perfectly matched counterparts. Approximately 10 min after initiation of the washing, the *NR* values for the CD 8/9 mutation site (Figs. 5a and 6b) stabilised above 0.8 and below 0.2 for the WT and MT targets, respectively. For the 1:1 mixed MT:WT target, the normalised ratio remained close to the value of 0.54 obtained before

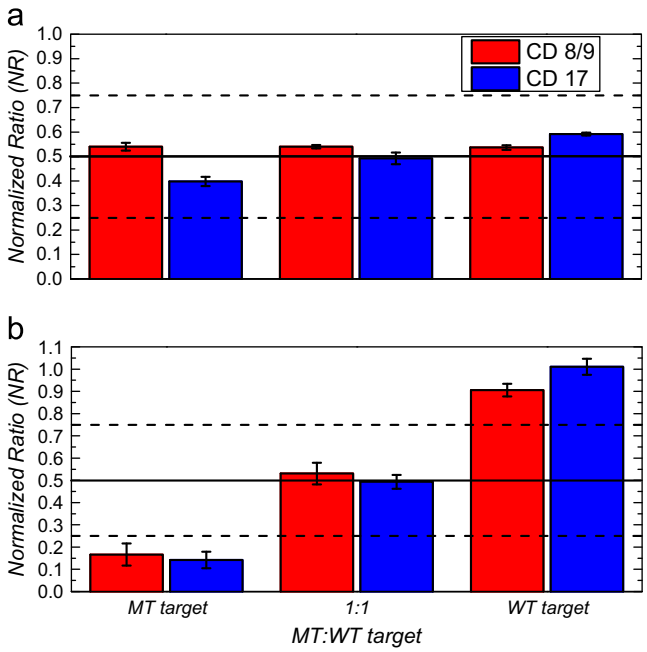

Fig. 6. Normalised ratio (*NR*) of sensors signals measured for different WT and MT target ratios. The experiments were performed with capture probes for the CD 8/9 and CD 17 mutation sites in the human HBB gene. The signals were measured (a) after 30 min incubation of the target and bead suspension on the sensor; and (b) 25 min (CD 8/9) or 2 min (CD 17) after washing in stringent buffer. Error bars are standard deviations obtained from repeated experiments ($n=3$).

washing. For the CD 17 mutation site (Figs. 5b and 6b), the maximum separation of the normalised ratios for the different targets was observed 2 min after initiation of the washing. For longer times, the separation was reduced and the standard deviation of the normalised ratio increased because of denaturation of both the mismatching and matching DNA duplexes, which resulted in a decrease of the sensor signals. For this mutation, the normalised ratio for the 1:1 mixed MT: WT target after washing assumed a value of $NR \cong 0.49(3)$.

4. Discussion

4.1. Characterisation of differential sensor

The study on the biotin-streptavidin bound beads on sensor surface showed the strengths and weaknesses of the two sensor designs. For both sensor designs, the signal due to bound beads was found to depend linearly on the number of functionalised sensor arms. The maximum signal from the dPHEB design was only half of the maximum signal from a PHEB design, because only half the sensor was used for sensing as the other sensor half was used as a local negative reference. However, the signals from the dPHEB design showed no offset both before and after washing when the sensor arms were not functionalised and the standard deviations of the sensor signals were about four times smaller than for the corresponding data for the PHEB sensors (Fig. 4). We speculate that due to the nearness of the sensing and reference arms of the dPHEB sensors, the two parts of the sensor are exposed to the nearly identical temperature, background bead concentration, external magnetic field and hybridisation conditions and that this results in the lower offset and variance of the signals. Therefore, the *environmental* parameters affecting the sensor are efficiently cancelled out in dPHEB sensors and these can be used to measure the amount of beads that are *specifically* bound to the top half of the sensor. For these reasons, the dPHEB sensors are the best choice for surface-based assays.

4.2. DNA hybridisation and dose-response curve

The design of the dPHEB sensors, and in particular the local reference, allowed for target detection in concentrations down to 156 pM, with a dynamic range of about two orders of magnitude and a low background. The obtained detection limit and dynamic range is well suited for analysis of DNA products from an amplification process such as polymerase chain reaction (PCR). Other research groups have been using magnetic labels for this purpose. In particular, Xu et al. (2008) demonstrated the detection of 10 nM of PCR products by adding magnetic particles to a spin valve sensor onto which the target was hybridised outside the measurement system. Our system offers a microfluidic liquid control as well as control of the sensor temperature during real-time measurements. These are key elements to carry out the hybridisation procedure on-chip. The integration of these control systems with the sensor allows for a real-time measurement of the hybridisation reaction.

The closest comparable method to the present one is DNA microarrays. Microarrays based on end-point fluorescence readout in a commercial microarray reader typically have detection limits of 1–10 pM. The detection limit depends on hybridisation time, surface chemistry, slide material, and the probes used. The fluorescence readout typically has several orders of magnitude of dynamic range. Non-fluorescent readouts, such as colorimetric enzymatic readouts, have detection limits similar to fluorescence (10–30 pM) but with only one or at most two orders of magnitude of dynamic range (Chen et al., 1998; Petersen et al., 2007). The present method has a higher detection limit and a dynamic range similar to colorimetric detection methods. Dynamic ranges of one to two orders of magnitude are sufficient for SNP genotyping (Petersen et al., 2007). As the detection limit for the presented method is high at present, it is better suited for analysis of targets prepared by an amplification process, such as PCR. The advantages of the presented method over optical detection are the integration in a compact microfluidic system with flexible reaction conditions and the ability to perform real-time measurements of the DNA hybridisation and dehybridisation.

Other chip-based methods to measure hybridisation in real-time includes surface plasmon resonance (SPR) (Auer et al., 2011), quartz crystal microbalance (QCM) (Wang et al., 2013), and film bulk acoustic resonators (FBAR) (Auer et al., 2011). These methods do not use a labelling of the targets and have detection limits of about 1 nM. This limit is set by the unspecific binding of the sample matrices to the sensor surface (Auer et al., 2011, Wang et al., 2013). Since there is virtually no magnetic signal from biological material, magnetic label detection is insensitive to the sample matrix. Moreover dPHEB sensors, via their integrated local negative reference, are effective in cancelling the signals from unspecifically bound targets and labels in suspension.

4.3. Real-time SNP genotyping

Stringent washing was employed to denature mismatched duplexes from the CD 8/9 and CD 17 mutations of the *HBB* gene. The same mutation sites were previously investigated by Petersen et al. (2009) under varying washing stringency conditions. In their work, an optimal washing buffer composition of $0.25 \times \mathrm{SSC} + 0.1\%$ SDS was identified for genotyping of the CD 8/9 mutation, but acceptable discrimination was obtained down to salt concentrations of $0.035 \times \mathrm{SSC}$. Here, we utilised $0.05 \times \mathrm{SSC} + 0.05\%$ SDS, which is within their working buffer range. For the CD 17 mutation site, Petersen et al. found that the optimal washing stringency was lower than that for the CD 8/9 mutation site, and that higher stringency conditions (i.e. washing at a lower salt concentration) led to lower reproducibility of the *NR* values due to loss of signal.

This agrees well with the results presented here, where the washing buffer was found to induce a fast denaturation of also the matched duplexes for the CD 17 mutation site. Nevertheless, with the dPHEB sensors, it was possible to perform real-time measurements during incubation and washing in contrast to the end-point detection employed in a standard microarray-based approach with fluorescence readout (Petersen et al., 2008, 2009; Poulsen et al., 2011). The real-time data can be used to obtain kinetic data and to optimise, for example, the timing of SNP genotyping. For both mutation sites, the value of *NR* changed rapidly after the washing was initiated (Fig. 5). For the CD 8/9 mutation site, the normalised ratio approached its equilibrium value after about 10 min and a clear distinction between a homozygote WT target (100% WT target) and a homozygote MT target (100% MT target) could be made using cut-off values of >0.75 and <0.25, respectively. For the CD 17 mutation site, the cut-off values were reached 2 min after initiation of the washing, after which the total signal decreased resulting in lower reliability of the values of *NR*. Considering the rapid signal change in Fig. 5, it is possible to perform a robust genotyping for the present samples just a few minutes after the high stringency buffer is introduced while longer washing times may reduce the total signal. Real-time data allows for genotyping of multiple SNPs even when the optimal washing time varies between different probe sets. Moreover, rapid SNP detection may be feasible using the presented approach.

5. Conclusions

A system for real-time hybridisation assays using magnetic labels and integrated magnetoresistive field sensors was described. The system comprised integrated microfluidic sample handling and temperature control. Each sensor included a local negative reference close to the active sensing area. Therefore, the influence of the sensor environment (temperature, external magnetic field, magnetic bead background) was strongly reduced. These features enabled real-time studies of the *specific* binding of magnetic beads to the upper part of the sensor in a background of magnetic beads under changing environmental conditions and strongly improved the reliability of the quantification of the specific binding of magnetic beads. In the system, we demonstrated the detection of DNA targets down to a concentration of about 160 pM. This number is anticipated to be further improved by optimising the sensor stack and geometry to achieve a higher sensitivity to surface-bound magnetic beads. Moreover, we demonstrated the strengths of the system in real-time SNP genotyping experiments on two mutation sites in the human *HBB* gene, where the hybridisation of WT, MT and a 1:1 mixture of WT and MT targets were monitored during incubation and stringent washing. The results showed data of high quality and reproducibility with a clear distinction between the three investigated targets for both investigated mutations.

The presented system provides a flexible tool for investigations of the real-time specific binding of magnetic beads to a functionalised sensor surface as function of biological target, the liquid composition and the temperature. Our future work aims at using this tool for studies of DNA hybridisation kinetics and for the optimisation of hybridisation conditions for SNP genotyping.

Acknowledgements

Frederik W. Østerberg acknowledges support from the Copenhagen Graduate School for Nanoscience and Nanotechnology (C:O:N:T) and the Knut and Alice Wallenberg (KAW) Foundation.

Appendix A. Supplementary material

Supplementary data associated with this article can be found in the online version at http://dx.doi.org/10.1016/j.bios.2013.09.026.

References

Auer, S., Nirschl, M., Schreiter, M., Vikholm-Lundin, I., 2011. Analytical and Bioanalytical Chemistry 400 (5), 1387–1396.
Chen, J.J.W., Wu, R., Yang, P.-C., Huang, J.-Y., Sher, Y.-P., Han, M.-H., Kao, W.-C., Lee, P.-L., Chiu, T.F., Chang, F., Chu, Y.-W., Wu, C.-W., Peck, K., 1998. Genomics 51 (3), 313–324.
Ejsing, L., Hansen, M.F., Menon, A.K., Ferreira, H.A., Graham, D.L., Freitas, P.P., 2004. Applied Physics Letters 84, 4729.
Er, T.-K., Chang, J.-G., 2012. Clinica Chimica Acta 414, 197–201.
Freitas, P.P., Ferreira, R., Cardoso, S., Cardoso, F., 2007. Journal of Physics: Condensed Matter 19, 165221.
Gaster, R.S., Hall, D.A., Nielsen, C.H., Osterfeld, S.J., Yu, H., Mach, K.E., Wilson, R.J., Murmann, B., Liao, J.C., Gambhir, S.S., Wang, S.X., 2009. Nature Medicine 15, 1327–1333.
Gaster, R.A., Hall, D.A., Wang, S.X., 2011. Nano Letters 11, 2579–2583.
Hansen, T.B.G., Damsgaard, C.D., Dalslet, B.T., Hansen, M.F., 2010. Journal of Applied Physics 107, 124511.
Henriksen, A.D., Dalslet, B.T., Skieller, D.H., Lee, K.H., Okkels, F., Hansen, M.F., 2010. Applied Physics Letters 97, 013507.
Howell, W.M., Jobs, M., Gyllensten, U., Brookes, A.J., 1999. Nature Biotechnology 17, 87–88.
Nørholm, M., Bruus, H., Jakobsen, M.H., Telleman, P., Ramsing, N.B., 2004. Lab-on-a-Chip 4, 28–37.
Østerberg, F.W., Dalslet, B.T., Snakenborg, D., Johansson, C., Hansen, M.F., 2010. AIP Conference Proceedings 1311, pp. 176–183.
Østerberg, F.W., Rizzi, G., de la Torre, Zardán Gómez, Strömberg, T., Strømme, M., Svedlindh, M., Hansen, M.F., P., 2013a. Biosensors and Bioelectronics 40 (1), 147–152.
Østerberg, F.W., Rizzi, G., Hansen, M.F., 2013b. Journal of Applied Physics 113, 234508.
Petersen, J., Stangegaard, M., Birgens, H., Dufva, M., 2007. Analytical Biochemistry 360 (1), 169–171.
Petersen, J., Poulsen, L., Petronis, S., Birgens, H., Dufva, M., 2008. Nucleic Acids Research 36, e10.
Petersen, J., Poulsen, L., Birgens, H., Dufva, M., 2009. PLoS One 4, e4808.
Poulsen, L., Søe, M.J., Møller, L.B., Dufva, M., 2011. PLoS One 6 (3), e14777.
Tamanaha, C.R., Mulvaney, S.P., Rife, J.C., Whitman, L.J., 2008. Biosensors and Bioelectronics 24, 1–13.
Wang, S.X., Li, G., 2008. IEEE Transactions on Magnetics 44, 1687–1702.
Wang, D., Chen, G., Wang, H., Tang, W., Pan, W., Li, N., Liu, F., 2013. Biosensors and Bioelectronics 48, 276–280.
Xu, L., Yu, H., Akhras, M.S., Han, S., Osterfeld, S., White, R.L., Pourmand, N., Wang, S.X., 2008. Biosensors and Bioelectronics 24 (1), 99–103.